J Neuropathol Exp Neurol

Vol. 68, No. 10
October 2009
pp. 1103–1115

ORIGINAL ARTICLE

Glutamatergic Reinnervation and Assembly of Glutamatergic Synapses in Adult Rat Skeletal Muscle Occurs at Cholinergic Endplates

Maura Francolini, PhD, Giorgio Brunelli, MD, Ilaria Cambianica, MSc, Sergio Barlati, PhD, Alessandro Barbon, PhD, Luca La Via, Bruno Guarneri, MD, Flora Boroni, PhD, Annamaria Lanzillotta, PhD, Cristina Baiguera, Michele Ettorre, PhD, Mario Buffelli, PhD, PierFranco Spano, PhD, Francesco Clementi, MD, and Marina Pizzi, PhD

Abstract

After denervation of adult rat abdominal muscles, the postsynaptic apparatus of neuromuscular junctions (NMJs) retains its original architecture and clustering of acetylcholine receptors (AChRs). When descending fibers of the spinal cord are surgically diverted to this muscle by a nerve grafting procedure, supraspinal glutamatergic neurons can innervate muscle fibers and restore motor function; the newly formed NMJs switch from a cholinergic to a glutamatergic-type synapse. We show here that regenerating nerve endings contact the fibers in an area occupied by cholinergic endplates. These NMJs are morphologically indistinguishable from those in controls, but they differ in the subunit composition of AChRs. Moreover, by immunofluorescence and immunoelectron microscopy, new NMJs express glutamatergic synapse markers. The α-amino-3-hydroxy-5-methyl-4-isoxazolepropionic acid (AMPA) receptor subunit GluR1 partially colocalizes with AChRs, and vesicular glutamate transporter 2 is localized in the presynaptic compartment. Immunoprecipitation analysis of membranes from reinnervated muscle showed that AMPA receptor subunits GluR1 and GluR2 coimmunoprecipitate with rapsyn, the AChR-anchoring protein at the NMJ. Taken together, these results indicate that cholinergic endplates can be targeted by new glutamatergic projections and that the clustering of AMPA receptors occurs there.

Key Words: Acetylcholine receptors, AMPA receptors, Glutamate, Neuromuscular junction, Reinnervation, Spinal cord injury, Synaptic plasticity.

INTRODUCTION

Bypassing a spinal cord lesion by connecting healthy descending motor fibers with skeletal muscle may represent a promising surgical approach for the treatment of paraplegia (1, 2). We recently demonstrated that axotomized rat glutamatergic supraspinal neurons can regrow in a peripheral nerve graft connected to the distal tip of the transected nerve of abdominal muscles where they target the muscle fibers and make functional synapses. The glutamatergic reinnervation specifies the type of postsynaptic receptor. Reinnervated muscle fibers express increased amounts of α-amino-3-hydroxy-5-methyl-4-isoxazolepropionic acid (AMPA) glutamate receptor subunits that cluster at the junctional postsynaptic site. At 2 months after nerve grafting, nerve-evoked contraction of the skeletal muscles becomes insensitive to curare but is efficiently blocked by the AMPA receptor antagonist GYKI 52466 (1).

When motor axons regenerate after peripheral nerve injury, the cholinergic terminals of regrowing motoneurons reoccupy precisely the original endplate sites (3, 4). When skeletal muscle is reinnervated by supraspinal glutamatergic neurons, however, it is not known whether the cholinergic apparatus is still preserved and whether regenerating glutamatergic axons reach the cholinergic endplates rather than new areas where the postsynaptic glutamatergic receptors are clustered. The possibility that functional AMPA receptors assemble at the cholinergic postsynaptic membrane recently became more plausible when glutamate receptors were immunolocalized at the neuromuscular junction (NMJ) of mouse quadriceps (5).

To investigate the presence of cholinergic endplates and the localization of newly formed glutamatergic synapses in rat abdominal muscles, we first analyzed the structure of NMJs in the internus obliquus and transversus abdominis

From the Department of Medical Pharmacology (MF, IC, FC), University of Milan and CNR Neuroscience Institute, Milan, Italy; Foundation for Experimental Spinal Cord Research (GB), Neurophysiology of the Spedali Civili of Brescia (BG), Division of Biology (SB, AB, LLV), and Pharmacology and Experimental Therapeutics (FB, AL, CB, PS, MP) of the Department of Biomedical Sciences and Biotechnologies, School of Medicine, University of Brescia, Brescia, Italy; and Department of Neurological and Vision Sciences, Section of Physiology (ME, MB), University of Verona, Verona, Italy.

Send correspondence and reprint requests to: Maura Francolini, Department of Medical Pharmacology, University of Milan, via Vanvitelli 32, 20129 Milan, Italy; E-mail: maura.francolini@unimi.it

This work was supported by grants from Ministero dell'Istruzione, dell'Università e della Ricerca, PRIN 2005, 2006, Centro di Studio e Ricerca sulla Terza Età, Brescia; Centro di Eccellenza per la Innovazione Diagnostica e Terapeutica, University of Brescia–Ministero dell'Istruzione, dell'Università e della Ricerca; Fondazione Monzino Milano.

Supplemental digital content is available for this article. Direct URL citations appear in the printed text and are provided in the HTML and PDF versions of this article on the journal's Web site (www.jneuropath.com).

muscles. Both denervated and muscle reinnervated by supraspinal neurons after the surgical grafting procedure displayed stable clusters of acetylcholine receptors (AChRs) at all times examined. We studied the ultrastructure of the newly formed neuromuscular synapses and demonstrated by immunoelectron microscopy that the NMJs in muscles surgically reconnected to the spinal cord by the nerve graft express markers of glutamatergic synapses. The AMPA receptors clustered at the postsynaptic membrane and partially colocalize with AChRs by interacting with anchoring proteins of the cholinergic postsynaptic apparatus.

MATERIALS AND METHODS

Surgical Procedure

All experimental and surgical procedures conformed to the National Research Council's *Guide for the Care and Use of Laboratory Animals* and were approved by the Animal Research Committees of the University of Brescia. In male adult Wistar rats, a laminectomy was performed to expose the T10–L1 cord segment. The dura mater was opened over 3 mm on the lateral aspect of the cord. Roots were gently retracted, and an incision 2 mm deep was made in the lateral funiculus of the right T11–T12 spinal cord with a no. 11 blade. A stump of a peripheral nerve 50 mm long from the sural nerve of the same animal was inserted 1.5 mm into the cord incision. The graft was secured by tying a 9–0 suture through the epineurium of the peripheral nerve and the dura mater. The motor nerve innervating the right internal abdominal oblique and transversus muscles was transected, and the distal stump (20 mm long) was anastomosed to the free end of the grafted nerve by an 11–0 nylon suture. Postoperative treatment with enrofloxacine (10 mg/kg per day) was carried out for 6 consecutive days.

At different time points (from 2 to 10 months) after graft implantation into the right lateral funiculus of the spinal cord, rats were monitored for muscle reinnervation and function by an electromyographic device (Nicolet Biomedical, Madison, WI). Rats were deeply anesthetized and mechanically ventilated. Control and reinnervated abdominal muscles were exposed, and compound muscle action potentials (CMAPs) were measured in response to direct nerve stimulation. Rats were injected with vecuronium (800 μg/kg, intravenously). Nerve stimulation and CMAP recordings in reinnervated and control muscles were performed 30 minutes after drug injection, as described (1). In 6 animals, oblique and transversus abdominis muscles were surgically denervated by resection of their motor nerve.

Immunofluorescence Analysis

Denervated muscles were dissected and observed 10 days and 1 and 2 months after surgery. On a small portion of the muscle (3 mm × 1 cm), AChR clusters were stained by immersion in a solution of tetramethylrhodamine-conjugated α-bungarotoxin (TRITC-BuTx; Molecular Probes, Eugene, OR), 15 μg/mL in PBS (0.8% NaCl, 0.02% KCl, 0.144% Na_2HPO_4, 0.024% KH_2PO_4), pH 7.4, for 30 minutes, washed in PBS, and fixed with 4% paraformaldehyde in phosphate buffer 120 mmol/L, pH 7.4, overnight at 4°C. Fixed muscles were teased into thin bundles containing 10 to 20 muscle fibers that were processed for immunofluorescence with monoclonal antibodies against synaptophysin (1:100, Sigma, St Louis, MO). Briefly, the bundles were immersed for 2 hours in blocking solution (5% horse serum, 1% bovine serum albumin, 1% Triton-X100 in PBS, pH 7.4); they were then incubated with the primary antibodies diluted as indicated in blocking solution overnight at 4°C, washed in PBS supplemented with 0.5% Triton-X100, and incubated with fluorescence labeled secondary antibodies diluted in the same buffer for 2 hours. After extensive washing, the samples were mounted on glass slides with Mowiol (Sigma-Aldrich).

Reinnervated and control muscles were dissected at different time points after surgery; NMJ-enriched areas were cut, incubated with TRITC-BuTx, and fixed with 4% paraformaldehyde. Fixed tissues were further divided into bundles of 10 to 20 fibers of approximately 5 to 7 mm; the surgical dissection of these samples from the whole muscle was done under the stereomicroscope in the area of the terminal arborization of the grafted nerves and were processed for immunofluorescence as described with antibodies against the GluR1 subunit of the AMPA glutamate receptor (1:200; Chemicon, Temecula, CA), the vesicular glutamate transporter 2 (1:2000; VGLUT2 Synaptic System, Goettingen, Germany), synaptosome-associated protein of 25 kd (1:100, SNAP-25; Sigma), and synaptobrevin (1:100; VAMP2 Synaptic Systems). Visualization was performed by confocal microscopy (BioRad MRC1024, Hempstead, UK) after labeling with Alexa 488 (1:100; Molecular Probes)- and Cy5 (1:100; Jackson ImmunoResearch, West Grove, PA)-conjugated secondary antibodies. The entire surface of the sample was surveyed and checked for the presence of positive labeling, and all the confocal images were acquired using the same settings to evaluate differences in staining intensities between control and reinnervated NMJs.

Transmission Electron Microscopy and Immunogold Labeling

For transmission electron microscopy (TEM) analysis, bundles of fibers from control and reinnervated muscles were briefly fixed by immersion in 4% paraformaldehyde in phosphate buffer (30 minutes), washed, and incubated with TRITC-BuTx, as previously described. Regions of the sample enriched in NMJs, as identified with BuTx staining, were reduced in size to small segments of 4 to 5 fibers of 1-mm length and were entirely examined. These samples were further fixed with 2% glutaraldehyde in cacodylate buffer and processed for TEM. Briefly, after fixation, the samples were postfixed with osmium tetroxide, rinsed, en bloc stained with 1% uranyl acetate in water, dehydrated, and embedded in epoxy resin (Epon 812; Electron Microscopy Science, Hatfield, PA); blocks were baked for 24 hours at 67°C. Rat hippocampus, used for the immunogold experiments, was fixed by immersion in 2% glutaraldehyde in cacodylate buffer and processed as described. Thin sections were obtained with an ultramicrotome (Reichert Ultracut E; Leica Microsystems, Vienna, Austria), stained with uranyl acetate and lead citrate, and examined with a

TABLE 1. Distribution of Glutamate Immunoreactivity in Presynaptic Terminals of Central Synapses, Reinnervated, and Control NMJs Junctions

Compartments	Observed Gold, ng	Observed Points (P)	LD Values (ng/P a_p)	Expected Gold, ne	RLI Values	χ^2 Values
Reinnervated NMJs						
Vesicles	116	805	14.41	65.11	1.78	39.77*
Axoplasm	139	2623	5.29	212.16	0.65	25.22†
Mitochondria	117	1171	9.99	94.71	1.23	5.24
Total	372	4599	8.08	372	1	70.23‡
Control NMJs						
Vesicles	15	527	2.84	21.07	0.72	1.74
Axoplasm	71	1952	3.63	78.05	0.91	0.63
Mitochondria	47	847	5.54	33.86	1.38	5.09
Total	133	3326	3.99	133	1	13.46
Hippocampal synapses						
Vesicles	1247	1273	97.9	983.62	1.26	70.52*
Axoplasm	184	586	31.34	452.79	0.4	159.56†
Mitochondria	68	81	8.39	62.58	1.08	0.469
Total	1499	1940	77.26	1499	1	230.549‡

A test for randomness was applied to vesicles, mitochondria, and axoplasm of reinnervated and control neuromuscular junctions (NMJs) and central excitatory synapses (Materials and Methods). The subcompartment surface areas were estimated stereologically by random superimposition of a 0.01 μm^2 square grid (a_p = 0.01 μm^2) on the micrographs and counting the number of intersections between the grid lines and each subcompartment. Labeling densities and relative labeling index were then estimated for every compartment, and the results were tested for randomness.

*Number of gold particles significantly higher than the expected value ($p < 0.001$).

†Number of gold particles significantly lower than the expected value ($p < 0.001$).

‡Distribution of gold particles significantly deviates from random ($p < 0.001$).

Philips CM10 TEM. For immunolabeling experiments, we applied the method described by Phend and colleagues (6) to tissue sections fixed in 2% glutaraldehyde and embedded in Epon epoxy resin, as previously indicated. Fixation with high-concentration glutaraldehyde and epoxy resin embedding have been reported to retain tissue glutamate and make it available for subsequent immunolocalization at the TEM level (7). Freshly cut thin sections of rat hippocampus and control and reinnervated muscles were collected on nickel grids, washed in Tris-buffered saline with Triton ([TBST] 0.05 mol/L Tris, pH 7.6, 0.9% NaCl, 0.1% Triton-X100) for 5 minutes and then incubated with an antiserum against glutamate (1:50,000; Sigma) in TBST overnight in a moist chamber. After extensive rinsing with TBST, pH 7.6, the grids are floated on top of drops of TBST, pH 8.2, and subsequently incubated with a secondary antibody conjugated to 12-nm gold particles diluted in TBST, pH 8.2 (1:50, Jackson ImmunoResearch), for 1 hour at room temperature (RT). The specificity of the rabbit antiserum against glutamate has been characterized and previously described (8, 9). According to the manufacturer's specifications, the antiglutamate antiserum does not cross-react with L-aspartate, L-glutamine, L-asparagine, and L-alanine but may cross-react with dipeptides containing glutamate in a carboxy-terminal position (i.e. Asp-Glu and Gly-Glu); however, the high working dilution of the antiserum (1:50,000) strongly suggests that it has high affinity and specificity for glutamate in our immunolabeling experiments. Immunostaining specificity was further evaluated by omitting the primary antiserum, by incubating the grids with nonimmune rabbit serum (1:50,000 in TBST, pH 8.2), and by preabsorption experiments in which the primary antiserum was exposed to an excess of antigen (10 mmol/L glutamate, for 5 hours at RT) (6) (Figure, Supplemental Digital Content 3, http://links.lww.com/NEN/A59).

TABLE 2. Primer Sequences Used for Semiquantitative PCR Analysis

Gene	Primer Sequence	Tm, °C
AChRα1	α1-F CAC CTA CCA CTT CGT CAT GCA G	60
	α1-R ATA AAA ACC TTC CGC ACC CAC T	
AChRγ	γ-F CAG CAA GTA CCT GAC CTT CCT CA	60
	γ-R CCT AAA GAG GAG TTC GCT TCG AG	
AChRε	ε-F GAA GAG CTG AGC CTG TAT CAC CA	60
	ε-R TGC CCA TCA ATA TTG TTT TCC AG	
β-actin	Act-F AAA TCG TGC GTG ACA TTA AAG AG	60
	Act-R GAG GGG CCG GAC TCA TCG TAC	

AChRα, AChRγ, and AChRε, acetylcholine receptor α, γ, and ε subunits; Tm, melt temperature.

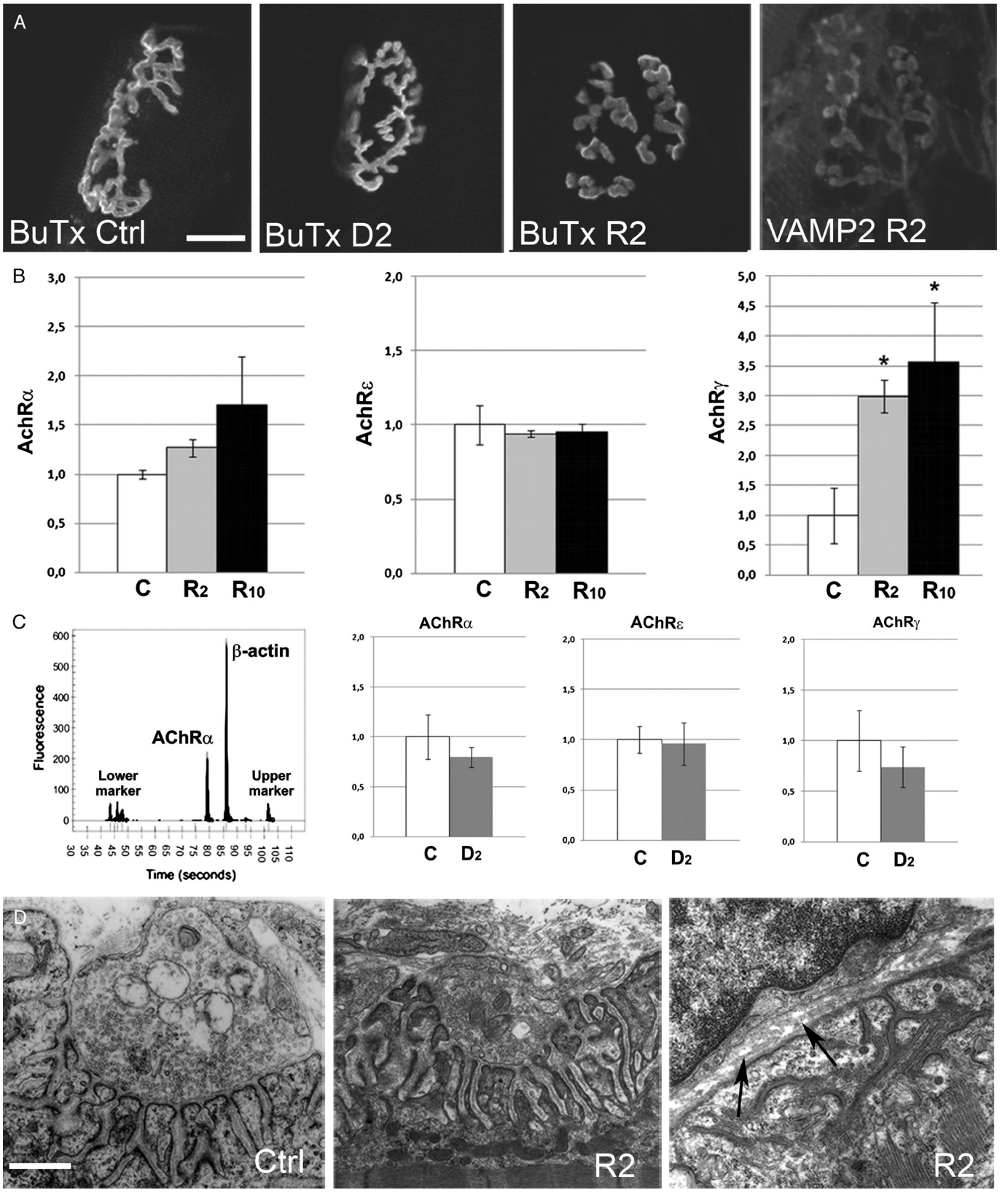

Image and Statistical Analysis

Gold particle densities were estimated by measuring the surfaces of presynaptic profiles (total surface of the bouton excluding the surfaces occupied by mitochondria) using National Institutes of Health Image software on TEM micrographs at a final magnification of 36,750×. We then manually counted the gold particles on these surfaces (gold particles lying on mitochondria were excluded), and the ratios between gold particle number and surface provided the density of gold particles expressed as number per square micrometer (7, 10). Statistical analysis of the density of glutamate-like immunoreactivity was evaluated with PRISM software using a 2-tailed unpaired *t*-test. The immunoelectron microscopy data were also analyzed with a test for randomness (11) to estimate the relationship between glutamate-like immunoreactivity and synaptic vesicle density in control and grafted NMJs and hippocampal synapses. To assess the degree of localization of glutamate, we defined 3 subcompartments of each presynaptic terminal: the pool of synaptic vesicles, the mitochondria, and the axoplasm. The basis of this statistical evaluation is to compare the expected distribution in each compartment according to a "random labeling" with the actual (observed) distribution of gold particles (11). Gold particles lying in each compartment (*observed gold* [ng]) were counted, a test grid lattice of 0.01 μm^2 (a_p) was applied onto the images, and each intersection of the grid to a specific subcompartment was determined to measure the compartment size (*observed points* [P]). The ratio *ng/P* a_p represents the labeling density (LD) of each compartment (gold particles per square micrometer). From the *observed points* of each individual compartment (P) and the ratio *total ng/total P*, the *expected gold* particle density (*ne = [P total ng/total P]*) that indicates the distribution expected if there were random or nonspecific labeling. For every compartment, the ratio *ng/ne* represented the relative labeling index (RLI).

The χ^2 values, calculated from the difference between observed and expected gold particles in each subcompartment $(ng\text{-}ne)^2/ne$, were used to assess statistical significance of the distribution of gold particles in the 3 subcompartments defined (Table 1).

Reverse Transcription–Polymerase Chain Reaction Analysis

Total RNA extracted from muscle specimens from regions enriched with nerve branches was analyzed by reverse transcription–polymerase chain reaction (RT-PCR) to identify the mRNA transcripts for AChR subunits. Different sets of primer pairs were used together with primers for β-actin, which was used as an internal standard (Table 2). An Agilent 2100 bioanalyzer was used for semiquantitative RT-PCR analysis (12).

Western Blot Analysis and Coimmunoprecipitation

Total protein extracts from portions of muscles that had received nerve branches were processed for Western blot analysis with antibodies against GluR1 (1:100; Chemicon), GluR2 (1:200; Chemicon); synapse-associated protein 97 ([SAP97] 1:1000; Affinity BioReagent, Inc, Golden, CO), glutamate transporter 1 (GLT1) (0.5 μg/mL), and glutamate aspartate transporter (GLAST) (0.5 μg/mL) gift of Dr Grazia Pietrini from the University of Milan, Italy (13), and βIII tubulin antibody (1:1500; Promega, Madison, WI). Homogenization was carried out by 10 strokes in a Teflon-glass homogenizer (700 rpm) in 4 mL/g of cold 0.32 mol/L sucrose containing 1 mmol/L HEPES, 1 mmol/L MgCl2, 1 mmol/L $NaHCO_3$, and 0.1 mmol/L phenylmethylsulfonyl fluoride (pH 7.4) in the presence of a complete set of protease inhibitors (Complete; Boehringer Mannheim, Mannheim, Germany) and phosphatase inhibitors. The homogenized tissue was centrifuged at 1,000 × *g* for 10 minutes. The resulting supernatant was centrifuged at 13,000 × *g* for 15 minutes to obtain a crude membrane fraction. The pellet was resuspended in 500 μL of buffer containing 1% digitonin, 50 mmol/L NaCl, 30 mmol/L triethanolamine, pH 7.5, 5 mmol/L EGTA,

FIGURE 1. (A) Analysis of neuromuscular junctions (NMJs) in control, denervated, and reinnervated muscle. The α-bungarotoxin (BuTx)–stained NMJs were observed by confocal microscopy; NMJ of control (BuTx Ctrl) rat abdominal muscles with its pretzel-like appearance and strong fluorescence staining of the TRITC-BuTx bound nicotinic acetylcholine receptors (AChRs). The general appearance of the NMJs is preserved 2 months after denervation (BuTx D2) and in the reinnervated muscle 2 months after the grafting procedures (BuTx R2). In reinnervated NMJs, the presynaptic terminals are again present as shown by the staining with a presynaptic marker VAMP2 (VAMP2 R2). Scale bars = 20 μm. **(B)** Reverse transcription–polymerase chain reaction analyses of AChR-α1, AChR-ε, and AChR-γ in control and reinnervated oblique muscles. The data were obtained by coamplification of β-actin and the different AChR transcripts in control (C) and reinnervated muscle 2 months (R2) or 10 months (R10) after nerve grafting. Data are mean ± SE of 3 rats per group examined in duplicate. **(C)** The RT-PCR analyses of AChR-α1, AChR-ε, and AChR-γ in control and denervated oblique muscles. An example electropherogram on the left traces β-Actin/AchR-α1 coamplification. Upper and lower markers are used as internal standards to eliminate sample-to-sample variation and to calculate size and concentration of each PCR product. The data were obtained by coamplification of β-actin and the different AChR transcripts in control **(C)** and denervated muscles at 2 months (D2). Histograms report the AChR/β-Actin ratio. Data are means ± SE of 2 rats examined in triplicate. Data were analyzed by Kruskal-Wallis nonparametric analysis of variance with adjustment for multiple comparisons. Value $p < 0.05$ was designated as significant. **(D)** Transmission electron microscopy shows that presynaptic terminals of control NMJs are filled with synaptic vesicles and mitochondria. They lay in deep primary folds on the muscle fibers and are covered by Schwann cells processes. The membrane of the muscle fiber is organized into secondary folds; a dense basal membrane occupies the synaptic cleft (Ctrl). In the grafted muscle, 2 months after surgery (R2, left), reinnervation is occurring and many fibers having completed the process with a normal appearance of presynaptic terminals; other fibers are still denervated as demonstrated by a lack of presynaptic nerve endings (arrows in R2, right). Scale bars = 500 nm.

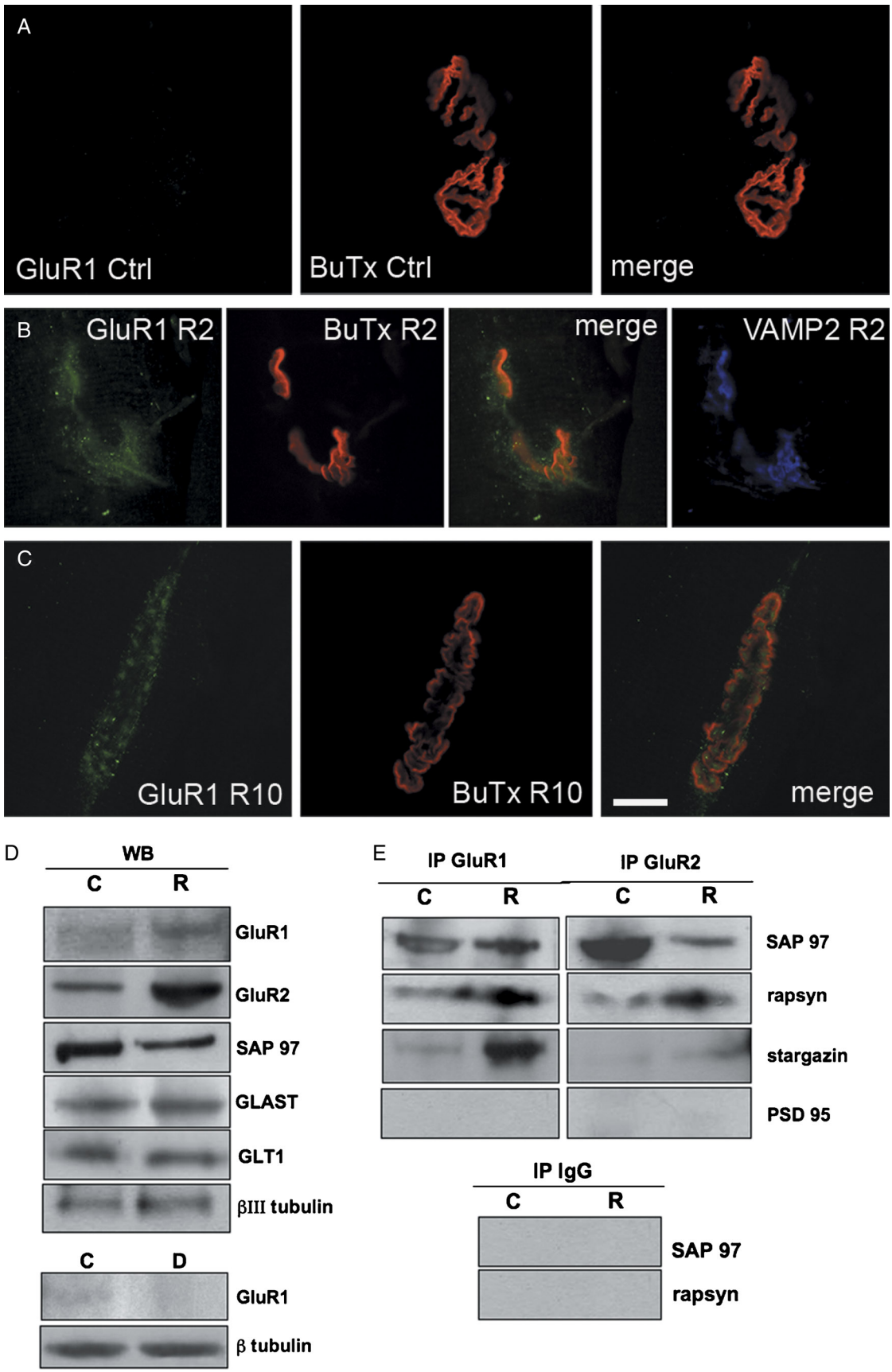

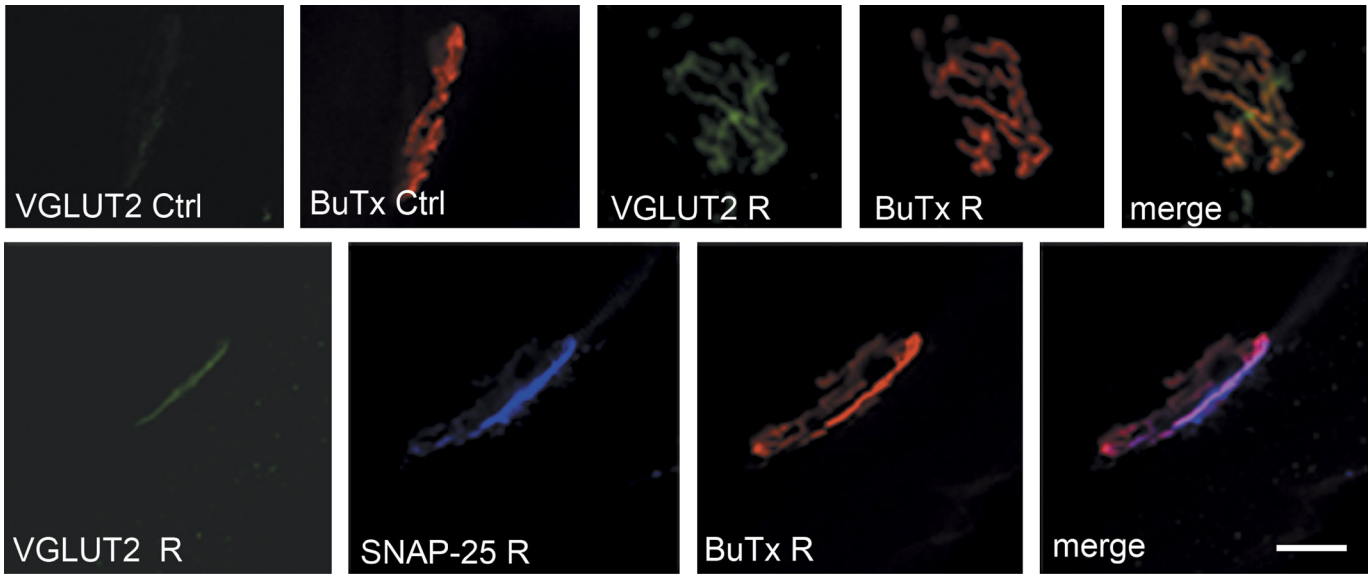

FIGURE 3. Localization of vesicular glutamate transporter 2 (VGLUT2) in neuromuscular junctions (NMJs) of reinnervated muscle. Control and reinnervated muscle were immunolabeled with antibodies against VGLUT2 at 2 months after surgery. In the NMJs of the control side (BuTx Ctrl), the signal for VGLUT2 is very faint (VGLUT2 Ctrl) (n = 91). In 33% of the NMJs of the reinnervated muscle (VGLUT2 R), labeling of the transporter is much higher and it colocalizes with BuTx (BuTx R) (n = 88). The lower panels show that in reinnervated NMJ, the presynaptic marker SNAP-25, visualized with a Cy5-conjugated secondary antibody (SNAP-25 R), colocalizes with VGLUT2 (VGLUT2 R) and with the postsynaptic marker BuTx (BuTx R). Scale bars = 20 μm

5 mmol/L EDTA, 50 mmol/L NaF, 2 mmol/L Na orthovanadate, 10 mmol/L *p*-nitrophenylphosphate, 50 μmol/L phenylarsine-oxide, 1 mmol/L benzamidine, 1 mmol/L *N*-ethylmaleimide, 1 mmol/L Na-tetrathionate, 1 mmol/L phenylmethylsulfonyl fluoride, 25 μg/mL aprotinin, and 25 μg/mL leupeptin, for 30 minutes on ice. To immunoprecipitate glutamate receptors, membrane proteins from muscle homogenates (20–30 μg) were incubated overnight at 4°C in modified radioimmunoprecipitation assay buffer (10 mmol/L tris-HCl, pH 8, 140 mmol/L NaCl, 0.5% [vol/vol] Nonidet P-40, 1 mmol/L sodium orthovanadate, 0.1% sodium dodecyl sulfate, 1 mmol/L phenylmethylsulfonyl fluoride, 1% protease inhibitor cocktail) with rabbit polyclonal antibodies against GluR1 (1:100; Chemicon) and GluR2 (1:200; Chemicon) or monoclonal anti-GluR1 (1:500 Santa Cruz Biotechnology, Santa Cruz CA) and anti-GluR2 (Chemicon). Normal rabbit IgG (Chemicon) was used as control antiserum. Protein A/G agarose beads were added, and samples were rotated for 2 hours at 4°C. The beads were washed, added to sodium dodecyl sulfate–polyacrylamide gel electrophoresis buffer, and boiled for 2 minutes. After centrifugation, supernatants were immunoblotted using the following antibodies: monoclonal anti-rapsyn (1:2000; Affinity BioReagents), anti-SAP97 (1:1000), anti-PSD95 (1:1000; Affinity BioReagents), and rabbit polyclonal anti-stargazin (1:1000; Upstate Biotechnology, Lake Placid, NY).

FIGURE 2. Glutamatergic markers in control and reinnervated neuromuscular junctions (NMJ). Control and reinnervated muscle samples were processed for immunofluorescence with antibodies against the glutamate receptor 1 (GluR1) subunit of the α-amino-3-hydroxy-5-methyl-4-isoxazolepropionic acid (AMPA) glutamate receptor; acetylcholine receptors (AChRs) were stained with α-bungarotoxin (BuTx). **(A)** The GluR1 is undetectable in control muscle (GluR1 Ctrl); BuTx fluorescence is very bright (BuTx Ctrl) (n = 168). **(B)** There is very clear labeling of GluR1 as well as the bright signal from BuTx (BuTx R2, GluR1 R2) in the reinnervated side 2 months after grafting; this was seen in about 10% of fibers. The fluorescent signals only partially overlap (merge), that is, a fraction of glutamate receptors are not associated with the AChR clusters. Reinnervation is confirmed by positive staining for VAMP (VAMP2 R2) (n = 167). **(C)** At 10 months after surgery, there is staining for GluR1 (GluR1 R10) and for AChRs (BuTx R10). Scale bars = 20 μm. **(D)** Western blot analysis (WB) of total extracts from control (C) and reinnervated (R) muscle with antibodies directed against GluR1, GluR2, synapse-associated protein 97 (SAP97), glutamate aspartate transporter (GLAST), and glutamate transporter 1 (GLT1). Membranes reprobed with antibodies against βIII-tubulin showed equal amounts of nerve terminals. No GluR1 was detected in 2 months' denervated (D) muscle. **(E)** Coimmunoprecipitation analysis of proteins interacting with GluR1 and GluR2 subunits in membrane extracts from control (C) and reinnervated (R) muscles. Extracts from membrane preparation were immunoprecipitated using anti-GluR1 or anti-GluR2 antibody. Precipitates were analyzed by immunoblotting using antibodies against SAP97, rapsyn, stargazing, and postsynaptic density 95 (PSD-95). A nonrelated antibody of the same isotype of antibody used for immunoprecipitation (IgG) did not immunoprecipitate SAP97 or rapsyn (lower panel), stargazin, or PSD-95 (data not shown). All biochemical assays were performed on extracts from 3 animals per experimental group; each experiment was repeated 3 times.

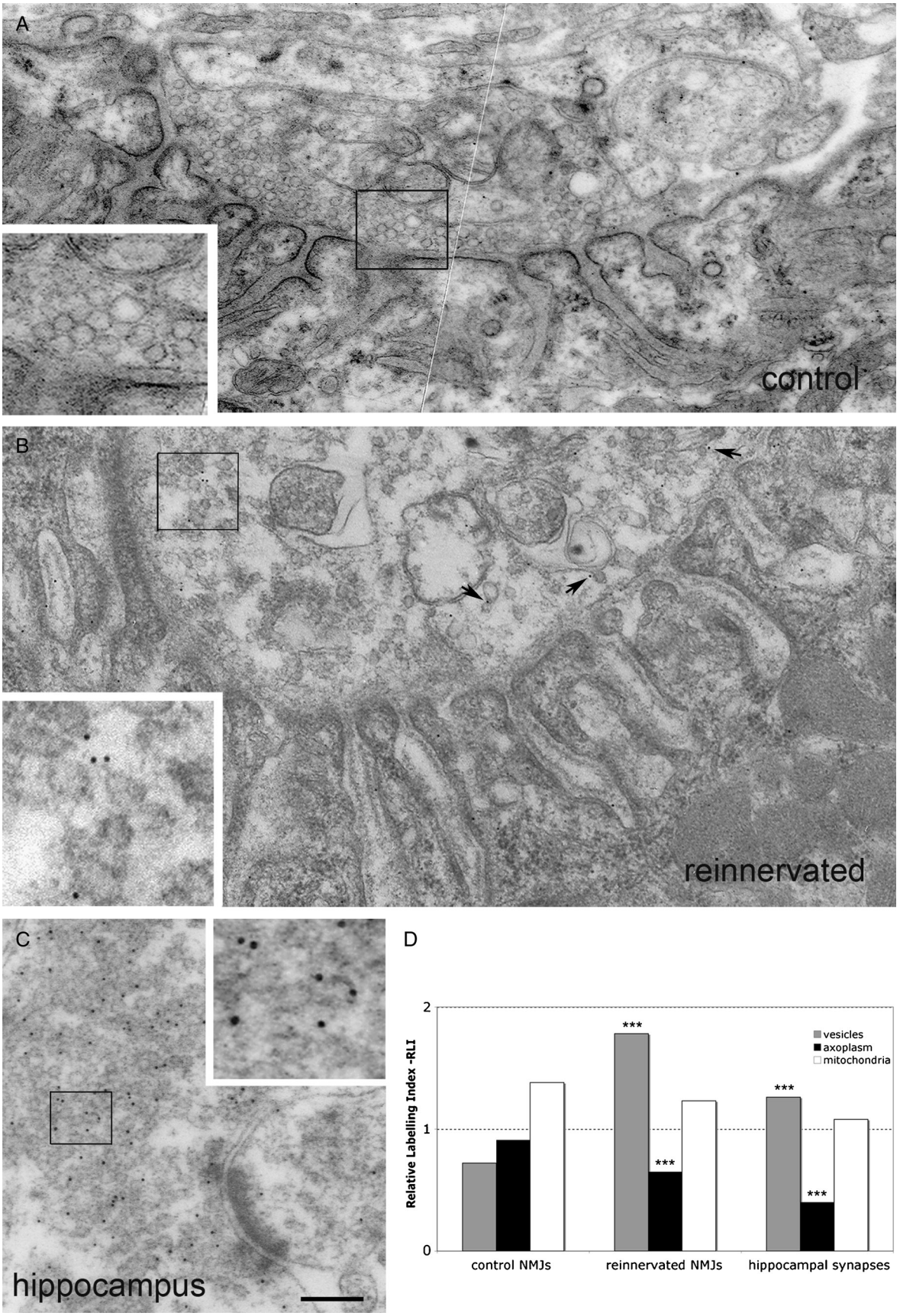

RESULTS

Persistence of AChR Clusters in Long-Term Denervated Muscle Fibers and in Muscle Reinnervated by the Nerve Grafting Procedure

Six rats were subjected to unilateral denervation of abdominal muscles; 21 rats were subjected to nerve-grafting procedures producing muscle reinnervation by supraspinal neurons, as previously described (1). The CMAP recording of muscle activity was performed in 16 rats, survived to the surgery, and reinnervated muscles were selected on the basis of their insensitivity to vecuronium. In 50% of the recorded muscles (i.e. in 8 rats), evoked CMAPs were sensitive to curare administration, indicating that muscles could undergo reinnervation by cholinergic sprouting either from the spinal cord or from collateral branching of adjacent, unaffected, cholinergic nerves; tissues from these animals were not considered in this study. Of the registered grafted muscles, 8 were considered as reinnervated by a noncholinergic innervation because they were resistant to vecuronium treatment (Figure, Supplemental Digital Content 1, http://links.lww.com/NEN/A57); these muscle fibers, hereafter referred to as *reinnervated fibers*, were dissected for further analysis.

Rat internal oblique and transversus muscles consist of a broad flat trapezoid abdominal muscle of about 2 × 3 cm. Nerve fibers innervating this muscle have broad terminal arborizations, and the NMJs are diffusely spread over the entire inner surface of the muscle where they form loose clusters. Tissue sampling was always from the area of terminal arborization of the grafted nerve into the muscle.

At 10 days or 1 and 2 months after denervation or 2 months after the grafting procedure, dissected muscle fibers were incubated with TRITC-BuTx to determine whether AChRs were still clustered in the postsynaptic membrane (Fig. 1A). In control muscle fibers, the NMJ showed a typical pretzel-like appearance and strong fluorescence staining of the AChRs bound by TRITC-BuTx. At 10 days and 1 (not shown) and 2 months after denervation, the general appearances of the NMJs were preserved, whereas the muscle itself underwent progressive atrophy. Lack of labeling with presynaptic markers confirmed the absence of nerve endings (not shown), thus confirming the effective denervation of the fibers. By fluorescence, the AChRs labeled with TRITC-BuTx were still present in the NMJs in the reinnervated muscles, and their organization was similar in size and shape to those in the control fibers. Reinnervation was confirmed by positive staining for presynaptic markers (VAMP2; Fig. 1A and Figure, Supplemental Digital Content 2, http://links.lww.com/NEN/A58, upper panel). By 2 months after nerve graft implantation, the reinnervated muscle recovered from atrophy.

Molecular Changes of Nicotinic Receptors in Reinnervated Motor Endplates

We then analyzed the expression of mRNAs that code for the nicotinic AChR subunits AChRα1, AChRε, and AChRγ (Fig. 1B). All the AChR mRNAs were expressed in both control and reinnervated muscles. No significant variation in expression level of AChRα1 and AChRε (which are contained in adult nicotinic AChRs) was evident in reinnervated muscles at 2 and 10 months after the grafting procedure. Conversely, the level of AChRγ mRNA (which is highly expressed in fetal motor endplates and during the early phase of muscle denervation) seemed stably increased in reinnervated muscle up to 10 months after the surgery. In corresponding 2-month denervated fibers, the levels of AChRα1, AChRγ, and AChRε mRNAs were comparable to those of control muscle (Fig. 1C).

Ultrastructural Analysis of Reinnervated NMJs

Presynaptic terminals in control NMJs laid in deep primary folds on the muscle fibers and were covered by Schwann cell processes (Fig. 1D, left panel). The membrane of the muscle fiber was organized into secondary folds, and a dense basal membrane occupied the synaptic cleft. In long-term denervated NMJs, the presynaptic nerve terminals were missing; the primary folds were flattened, whereas the architecture of the secondary folds was maintained. Muscles with progressive atrophy accumulated connective tissue heavily (not shown). At 2 months after nerve grafting, most of the endplates were still denervated, as demonstrated by a lack of presynaptic terminals and by flattening of the primary folds; the secondary folds were preserved (Fig. 1D, right

FIGURE 4. Ultrastructural immunolocalization of glutamate in control and reinnervated neuromuscular junctions (NMJs) and hippocampus. Thin sections of fibers from control and reinnervated abdominal muscles were immunolabeled with an antibody against glutamate and then visualized by electron microscopy (EM) with a secondary antibody conjugated to 12 nm gold particles. In control muscle **(A)**, the NMJ shows only faint labeling; NMJs of the reinnervated muscle **(B)** show a higher number of gold particles in every presynaptic profile examined; these gold particles are closely associated with synaptic vesicles (arrows and inset). **(C)** Sections of rat hippocampus were similarly immunolabeled with the antiglutamate antibody and visualized by EM; the glutamatergic synapse is strongly labeled, and gold particles are in close association with synaptic vesicles (inset). Scale bars = 250 nm. **(D)** Test for randomness was applied to evaluate the distribution of glutamate in hippocampal synapses (n = 15), control (n = 18), and reinnervated NMJs (n = 16). The labeling densities (Table 1) and relative labeling index (RLI) were estimated for each compartment, and the results were tested for randomness (χ^2 analysis). The histogram of the RLI of the 3 subcompartments (vesicles, axoplasm, mitochondria) that constitute the presynaptic terminals of control and reinnervated NMJs and of hippocampal synapses shows that the RLI of the vesicles pool in reinnervated NMJs and hippocampal synapses are similar and differ significantly from random distribution (RLI > 1; $p < 0.001$), indicating that this compartment is preferentially labeled. By contrast, the RLI of the soluble component (axoplasm) in both cases is lower than 1 ($p < 0.001$), indicating that glutamate is not present in this compartment. The mitochondrial pool RLI is higher than 1 (Table 1) in reinnervated and control NMJs (RLI, 1.23 and 1.38, respectively) and in hippocampal synapses (RLI, 1.08); this could be the results of the localization of metabolic glutamate inside these organelles and/or the result of the interaction of the antibody with some Krebs cycle intermediates (i.e. succinate) (6).

panel). In reinnervated muscles, however, the presynaptic terminals had a normal phenotype and the postsynaptic apparatus recovered its original architecture (Fig. 1D, center panel). At 10 months after surgery, the NMJs showed an increase in the percentage of reinnervating fibers, and the presynaptic terminals and postsynaptic specializations were identical to those of control NMJs (not shown). Ultrastructural analysis of reinnervated muscles did not show presynaptic terminals that contacted the surface of the muscle fibers in the absence of the postsynaptic specializations typical of cholinergic endplates.

Newly Formed NMJs Exhibit Markers of Glutamatergic Synapses

Because after the grafting procedure the abdominal muscles undergo a functional glutamatergic reinnervation (1), we analyzed expression of the characteristic proteins of central glutamatergic synapses by the NMJs in control (contralateral) and reinnervated tissues from 7 animals by immunofluorescence. Figure 2A shows the staining pattern of an NMJ in control muscle. The GluR1 is undetectable, whereas the BuTx fluorescence of the AChRs is present and well defined (control NMJs examined, n = 168). On the grafted side 2 months after surgery, approximately 10% of the muscle fibers displayed clear labeling of GluR1 in combination that partially overlapped with the signal obtained from BuTx (Fig. 2B) (reinnervated NMJs examined, n = 167). These NMJs were effectively reinnervated as demonstrated by staining with a presynaptic marker (VAMP2); in no cases were there clusters of GluR1 immunoreactivity that were not associated with BuTx. Similar results were obtained in muscle examined at 10 months after the surgery (Fig. 2C). The positive labeling for GluR1 was absent in NMJs of muscles that underwent reinnervation by cholinergic input (Figure, Supplemental Digital Content 2, http://links.lww.com/NEN/A58, lower panel), as demonstrated by the sensitivity of muscle contraction to vecuronium administration.

Vecuronium-insensitive and control muscles were immunolabeled with antibodies against the VGLUT2 (Fig. 3). In the NMJs of the control side, the signal for the transporter was very faint (control NMJs examined, n = 91), whereas in 33% of the NMJs of the reinnervated muscles, the labeling for the transporter was much higher and aligned with the profile of the postsynaptic apparatus (reinnervated NMJs examined, n = 88). Moreover, in reinnervated NMJs, the staining for VGLUT2 colocalized with the ubiquitous presynaptic marker SNAP-25; both signals overlapped the staining of AChRs in the postsynaptic membrane. These data indicate that new GluR1 subunits accumulate at the postsynaptic specialization of muscle reinnervated by glutamatergic axons and that these proteins are stably inserted in the clusters of AChRs or in close proximity to them.

To verify interactions of GluRs with anchoring molecules at the cholinergic postsynaptic apparatus or scaffolding proteins critical at synapses in the central nervous system but also localized at the skeletal NMJ (14), we performed immunoblot analysis on muscle total extracts (Fig. 2D) and membrane preparations (Fig. 2E) of control, denervated, and reinnervated muscle. Both GluR1 and GluR2 were detected (albeit at very low levels) in control muscles enriched with βIII tubulin-positive nerve terminals. As previously shown (1), the levels of GluR1 and GluR2 subunits increased in total tissue extracts of reinnervated muscle. No GluR1 protein was found in corresponding 2-month denervated muscle. Consistent with previous immunolocalization of GLT1 and GLAST at postsynaptic membrane of rat NMJs (15), we detected GLT1 and GLAST proteins in tissue extracts with no apparent difference between control and reinnervated muscles. Moreover, tissue extracts were positive for SAP97, a member of the membrane-associated guanylate kinases that have a key role in the cerebral regulation of AMPA receptor trafficking and are expressed in NMJs (5, 14). The content of SAP97 was reduced in reinnervated muscle (Fig. 2D). Coimmunoprecipitation analysis of proteins interacting with GluR1 and GluR2 was then performed in membrane preparations (Fig. 2E). In reinnervated muscle, antibodies to both GluR1 and GluR2 highly coimmunoprecipitated rapsyn, the muscle protein anchoring AChRs at the postsynaptic membrane and which is essential for its clustering at NMJs (16). Likewise, rapsyn and stargazin, the AMPA receptor–interacting protein at brain postsynaptic densities (17), coprecipitated with GluR1 and to a lesser extent with the GluR2 subunit in reinnervated muscle. In addition, large amounts of SAP97, but not PSD-95, were detected in GluR immunoprecipitates. None of those proteins was present in immunoprecipitates performed with unrelated antibodies (Fig. 2E).

Glutamate-Like Immunoreactivity in Reinnervated NMJs

Thin sections of rat hippocampus and control and reinnervated muscles from 3 animals were immunolabeled with an antibody against glutamate and then visualized at the TEM level with a secondary antibody conjugated to 12-nm gold particles. There was only slight labeling in a typical control NMJ (Fig. 4A and inset), whereas NMJs of the reinnervated muscle showed more numerous gold particles in every presynaptic profile examined (Fig. 4B); the particles were closely associated with synaptic vesicles (Fig. 4B inset). Sections of rat hippocampus were used as a positive control for the labeling (Fig. 4C); in these sections, glutamatergic presynaptic terminals were labeled by the antiglutamate antibody, and the gold particles were observed in close association with synaptic vesicles (Fig. 4C inset). Gold particle densities were determined in presynaptic terminals of control NMJs (2.9 ± 0.45 particles/μm^2, n = 18), reinnervated NMJs (6.72 ± 0.70 particles/μm^2, n = 16), and hippocampal synapses (75.1 ± 7.82 particles/μm^2, n = 15). Gold particle densities between NMJs of control and reinnervated muscle were significantly different (unpaired *t*-test, $p \leq 0.001$). We then tested the distribution of glutamate immunoreactivity by evaluating the RLI of each of 3 subcompartments of the presynaptic terminals of central excitatory synapses, control and reinnervated NMJs. We defined the subcompartments as 1) synaptic vesicle pool, 2) mitochondrial pool, and 3) axoplasm. For each subcompartment, we calculated the labeling density and compared the

RLI (ratio between the number of observed gold particles and the expected number according to a random distribution) (Table 1). This test clearly shows that in reinnervated NMJs as well as in hippocampal excitatory synapses, the RLI of the synaptic vesicle compartment was significantly higher than expected according to a random distribution ($\chi^2 = 39.77$ and 72.61, respectively; $p \leq 0.001$), whereas the axoplasm compartment RLI was lower ($\chi^2 = 25.22$ and 158.25, respectively; $p \leq 0.001$). In control cholinergic NMJs, the RLI of each compartment examined do not significantly deviate from random distribution (Table 1; Fig. 4D). All immunolocalization data derived from 3 independent experiments in which freshly cut thin sections of 2 blocks of hippocampus and at least 10 different resin blocks each for control and reinnervated muscle were processed. Because the NMJs of abdominal muscle are dispersed in loose clusters, every block of muscle tissue (4–5 fibers, 1 mm in length) contains at most 1 or 2; in reinnervated muscle, some of them might have still been denervated and thus not usable for this analysis.

DISCUSSION

Connecting the distal stump of the transected nerve of abdominal muscles with the lateral bundle of rat spinal cord by a peripheral nerve graft results in functional muscle reinnervation (1). Reinnervation occurs by axonal elongation of glutamatergic supraspinal neurons originating from rubrospinal, reticulospinal, and vestibulospinal tracts (1). Reinnervated muscle becomes insensitive to classical nicotinic receptor antagonists but sensitive to selective blockers of glutamate AMPA receptor subtypes (1, 2). The present results expand on previous evidence showing that by switching from the cholinergic to the glutamatergic input, the postsynaptic cholinergic apparatus does not disappear and new clusters of AMPA receptors colocalize with AChRs.

Acetylcholine is the neurotransmitter operating at the mammalian NMJ, but glutamate may participate in modulating cholinergic transmission. This is suggested by the finding that presynaptic terminals of rodent NMJs are positive for glutamate labeling (10, 18). Glutamate release contributes to the maintenance of the resting membrane potential (19) and inhibits the nonquantal release of ACh from nerve terminals (20). Released glutamate would exert its effects through the activation of postsynaptic *N*-methyl-d-aspartic acid receptors, mainly in Type II muscle fibers (21, 22), via nitric oxide regulation of the chloride transporter (23) or alternatively through interaction with metabotropic glutamate receptors, as described for frog NMJs (24). Recently, the presence of the NR1 and NR2 subunits has been reported along with the subunits GluR1 and GluR2/3 of the AMPA receptor subtype in quadriceps muscles of young mice (5). The precise localization of glutamate in presynaptic terminals remains elusive, however, since to date, even immunogold experiments failed to demonstrate its association with synaptic vesicles (10). Data supporting the presence of vesicular glutamate transporters at NMJs are rather scant. Rat spinal motoneurons express VGLUT1 and VGLUT2, but these proteins are confined at terminals contacting Renshaw inhibitory interneurons and are not present at neuromuscular synapses (25). The VGLUT1-positive NMJs are found in striated esophageal muscle but not in other mouse muscle types (26), and all muscle types were negative for VGLUT2 and 3 immunoreactivity. Although VGLUT3-like immunoreactivity in close proximity to the NMJs of rat muscle tissue was reported (27), recent electrophysiological experiments failed to demonstrate the contribution of glutamate in neurotransmission at mammalian NMJs (28).

Immunofluorescence experiments in the present study confirmed that connecting the distal stump of abdominal muscles nerve with the lateral bundle of rat spinal cord produces a glutamatergic re-innervation of abdominal muscles. Grafted nerve terminals expressed high levels of VGLUT1 and VGLUT2 as previously demonstrated by Western blot analysis of nerve-muscle templates (1). Approximately 30% of the presynaptic terminals of NMJs in reinnervated muscles were strongly labeled with antibodies against VGLUT2. This staining colocalizes with other ubiquitous presynaptic markers, thus indicating that nerve terminals have the machinery to load glutamate into synaptic vesicles. Immunogold experiments at the TEM level provided corroborating evidence that in the presynaptic terminals of re-innervated NMJs, the glutamate content is significantly higher than in control NMJs. Stereological analysis demonstrated that glutamate is not dispersed in the axoplasm, but is associated with the synaptic vesicle pool. The density of glutamate labeling in presynaptic vesicles of reinnervated NMJ seemed lower than that observed in control hippocampal sections. This might be a consequence of a lower concentration of glutamate at the presynaptic terminals of regenerating supraspinal neurons or may have been the result of the glutamate release from presynaptic terminals in response to repeated nerve stimulation during the electromyographic analysis of re-innervation. In addition, diverse fixation procedures (see Materials and Methods and Appendix) may be responsible for different retention of neurotransmitter in the 2 templates. The TEM immunolocalization of glutamate together with immunolocalization of VGLUT2 in presynaptic terminals of re-innervated NMJs strongly indicate that, as in central excitatory synapses, in reinnervated NMJs glutamate is contained in synaptic vesicles and may be released upon stimulation in a quantal manner.

It is established that at the postsynaptic membrane of cholinergic NMJ, the number and lifetime of AChRs are maintained by innervation because receptors are destabilized after denervation or block of synaptic transmission (3, 29–32). The clusters of AChRs never disappear (33), but a decrease in endplate AChRs has been described in some muscle types of young adults (34). In adult muscle fibers, junctional AChRs are composed of 4 different subunits with a stoichiometry of $\alpha 2\beta\varepsilon\delta$, whereas there is insertion of fetal γ subunit of AChRs in place of ε in either junctional or extrajunctional regions in denervated ones (35). In denervated muscle, the insertion of AChRs into the membrane is preceded by upregulation of mRNA for all the subunits (35, 36). The AChR mRNAs return to control level 2 months after denervation (37, 38) or earlier if the denervated muscle is stimulated electrically (35) or reinnervated (37). Reinnervation by cholinergic neurons restores the morphological and

functional features of the original endplate (39). We found that after glutamatergic reinnervation, AChR clusters persist in muscle fibers for 10 months after the surgery. This reinnervation did not significantly affect AChRα and AChRε subunit expression but was associated with a stably increased level of AChRγ subunit. As occurring after cholinergic reinnervation (40), we did not observe major morphological alterations within the postsynaptic apparatus either by BuTx fluorescence or by TEM in the reinnervated muscle fibers. Further analysis of postsynaptic apparatus revealed a strong positivity for the AMPA glutamate receptor GluR1 in muscles reinnervated by glutamatergic fibers, thus confirming previous biochemical and immunofluorescence data (1). Interestingly, the newly assembled glutamatergic synapses colocalized with the cholinergic endplate areas, suggesting that signals guiding the growth of cholinergic spinal motor axons after nerve injury can also guide the regrowth of axons from glutamatergic supraspinal neurons. No clustering of glutamate receptors was detected outside the AChR-stained NMJs. Indeed, the cholinergic postsynaptic apparatus and AMPA receptors not only colocalized by immunofluorescence analysis, but also coimmunoprecipitated in biochemical assays. Coimmunoprecipitation assays in membrane preparations from reinnervated muscles showed that GluR1 and GluR2 subunits interacted with both stargazin, a scaffolding protein of the brain postsynaptic density-regulating AMPA receptor targeting the synaptic membrane (17, 41), and rapsyn, the AChR-anchoring protein at the postsynaptic apparatus of NMJs. This phenomenon may be related to a new synthesis of GluRs in response to the glutamatergic input or, more likely, to an increased synthesis of GluRs already expressed at the cholinergic postsynaptic membrane. Although we were unable to detect an immunofluorescence signal for GluRs in control NMJ of rat abdominal muscles, we cannot exclude the possibility that they are present at a very low density.

We previously found that normal muscle fibers constitutively express mRNAs for GluR1 to 4 and, more relevantly, that expression of GluR1 to 2 mRNAs displayed a trend to increase in muscles reinnervated by glutamatergic fibers (1). In addition, even if at low levels, GluR1 and GluR2 proteins, together with GLT1 and GLAST, were detected by immunoblot analysis in specimens of control muscles enriched with nerve terminals. Both GluR1 and GluR2 coimmunoprecipitated with rapsyn. The hypothesis that all the components of glutamatergic system are present in cholinergic NMJ is also supported by a recent study showing that GluR1 and GluR2/3 subunits along with NR1 and NR2 proteins immunolocalize at the postsynaptic membrane of mouse quadriceps (5). Differences related to the expression level of receptor subtypes may exist among diverse animal species and muscle types, as suggested by the lack of NR1 protein and transcript we reported in rat abdominal muscles (1). It has been shown that postsynaptic membranes in skeletal muscle fibers can also express PDZ domain-containing proteins SAP97 (5, 14, 42) and PSD-95 (14). We found that GluR1 and GluR2 were associated with SAP97, the key regulator of synaptic AMPA receptor trafficking at the brain postsynaptic densities. The interaction was evident in either control or reinnervated muscles. The interaction of GluRs with SAP97 dramatically decreased in muscles upon glutamatergic reinnervation. This suggests that under glutamatergic input, AMPA receptors are stably inserted at the NMJ membrane and that SAP97 dissociates from them, as commonly occurs in central glutamatergic synapses after AMPA receptors are stably transferred at the postsynaptic membrane (43). In addition, no interaction of PDS-95 with GluRs was detected; this is in line with evidence that PSD-95 does not directly bind to AMPA receptors and only slightly coprecipitates with GluRs (44). These results corroborate the idea that molecules specifically involved in intracellular transport, synaptic targeting, and anchoring of AMPA receptors in the brain synapses are also present at the NMJ (5, 42) and that they operate in response to changes of AMPA receptor expression.

It has been shown recently in cultures of chick neural tubes that selection of neurotransmitter phenotype in vertebrate motor neurons depends on specific calcium spike activity during embryonic neuronal development and that perturbing these endogenous calcium oscillations may result in a shift from acetylcholine to glutamate neurotransmitter phenotype (45). During early embryonic development, the muscle itself expresses mRNA and proteins of several neurotransmitter receptors including glutamate, GABA, and glycine; these mRNAs and proteins are subsequently downregulated to achieve the cholinergic phenotype of the mature NMJ. In vitro experiments show that modifying the neurotransmitter of motor axons induces alterations in receptor expression on muscle fibers to ensure the correct transmitter-receptor matching at the NMJ (46), a phenomenon with possible relevant implications for repair in mature nervous systems (47). Accordingly, we demonstrate that adult rat motor endplates, committed to receive a cholinergic input and expressing high levels of AChRs, nonetheless, retain the ability to express glutamate receptors (1). They can shift from a cholinergic to a glutamatergic phenotype in response to presynaptic glutamatergic input by increasing glutamate receptor expression to guarantee the appropriate neurotransmitter-receptor matching. The AChR clusters, however, remain in place and colocalize with glutamate receptors, suggesting that signals from the synaptic basement membrane in concert with factors released from regrowing fibers (48) can maintain AChR clusters while driving new synaptic differentiation.

ACKNOWLEDGMENTS

The authors thank Dr G. Pietrini (University of Milan) for the GLT and GLAST antibodies and Prof A. Cangiano (University of Verona) and Prof P. Mantegazza (University of Milan) for the constructive discussion and their helpful suggestions. The authors also thank Dr V. Cappello and M. Orlando for their skillful assistance with the electron microscopy experiments.

REFERENCES

1. Brunelli G, Spano P, Barlati S, et al. Glutamatergic re-innervation through peripheral nerve graft dictates assembly of glutamatergic synapses at rat skeletal muscle. Proc Natl Acad Sci U S A 2005;102:8752–57
2. Pizzi M, Brunelli G, Barlati S, et al. Glutamatergic innervation of rat skeletal muscle by supraspinal neurons: A new paradigm in spinal cord injury. Curr Opin Neurobiol 2006;16:323–28

3. Rich MM, Lichtman JW. In vivo visualization of pre- and postsynaptic changes during synapse elimination in re-innervated mouse muscle. J Neurosci 1989;9:1781–805
4. Wang S, Kawabuchi M, Zhou CJ, et al. The spatiotemporal characterization of endplate reoccupation, with special reference to the superimposition patterns of the presynaptic elements and the postsynaptic receptor regions during muscle re-innervation. J Peripher Nerv Syst 2004;9:144–57
5. Mays TA, Sanford JL, Hanada T, et al. Glutamate receptors localize postsynaptically at neuromuscular junctions in mice. Muscle Nerve 2009;39:343–49
6. Phend KD, Weinberg RJ, Rustioni A. Techniques to optimize post-embedding single and double staining for aminoacid neurotransmitters. J Histochem Cytochem 1992;40:1011–20
7. Storm-Mathisen J, Ottersen OP. Immunocytochemistry of glutamate at the synaptic level. J Histochem Cytochem 1990;38:1733–43
8. Hepler JR, Toomim CS, McCarthy D, et al. Characterization of antisera to glutamate and aspartate. J Histochem Cytochem 1988;36:13–22
9. Olivier E, Corvisier J, Pauluis Q, et al. Evidences for glutamatergic tectotectal neurons in the cat superior colliculus: A comparison with GABAergic tectotectal neurons. Eur J Neurosci 2000;12:2354–66
10. Waerhaug O, Ottersen OP. Demonstration of glutamate-like immunoreactivity at rat neuromuscular junctions by quantitative electron microscopy immunocytochemistry. Anat Embryol 1993;188:501–13
11. Mayhew TM, Lucocq JM, Griffiths G. Relative Labelling Index: A novel stereological approach to test for non-random immunogold labelling of organelles and membranes on transmission electron microscopy thin sections. J Microsc 2002;205:153–64
12. Gottwald E, Muller O, Polten A. Semiquantitative reverse transcription-polymerase chain reaction with the Agilent 2100 Bioanalyzer. Electrophoresis 2001;22:4016–22
13. Perego C, Vanoni C, Bossi M, et al. The GLT-1 and GLAST glutamate transporters are expressed on morphologically distinct astrocytes and regulated by neuronal activity in primary hippocampal cocultures. J Neurochem 2000;75:1076–84
14. Huang YZ, Wang Q, Won S, et al. Compartmentalized NRG signaling and PDZ domain–containing proteins in synapse structure and function. Int J Dev Neurosci 2002;20(3–5):173–85
15. Rinholm JE, Slettalokken G, Marcaggi P, et al. Subcellular localization of the glutamate transporters at the neuromuscular junction in rodents. Neuroscience 2007;145:571–91
16. Sanes JR, Lichtman JW. Induction, assembly, maturation and maintenance of a postsynaptic apparatus. Nat Rev Neurosci 2001;2:791–805
17. Chen L, Chetkovich DM, Petralia R-S, et al. Stargazin regulates synaptic targeting of AMPA receptors by two distinct mechanisms. Nature 2000; 408:936–43
18. Maister B, Arvidsson U, Zhang X, et al. Glutamate transporter mRNA and glutamate-like immunoreactivity in spinal motoneurones. NeuroReport 1993;5:337–40
19. Urazaev AK, Naumenko NV, Nikolsky EE, et al. The glutamate and carbachol effects on the early post-denervation depolarization in rat diaphragm are directed towards furosemide-sensitive chloride transport. Neurosci Res 1999;33:81–86
20. Malomouzh AI, Mukhtarov MR, Nikolsky EE, et al. Glutamate regulation of non-quantal release of acetylcholine in the rat neuromuscular junction. J Neurochem 2003;85:206–13
21. Berger UV, Carter RE, Coyle JT. The immunocytochemical localization of N-acetylaspartyl glutamate, its hydrolyzing enzyme NAALADase and the NMDAR-1 receptor at a vertebrate neuromuscular junction. Neuroscience 1995;64:847–50
22. Grozdanovich Z, Gossrau R. Co-localization of nitric oxide synathase I (NOS I) and NMDA receptor subunit 1 (NMDAR1) at the neuromuscular junction in rat and mouse skeletal muscle. Cell Tissue Res 1998;291:57–63
23. Vyskocil F. Early postdenervation depolarization is controlled by acetylcholine and glutamate via nitric oxide regulation of the chloride transporter. Neurochem Res 2003;28(3,4):575–85
24. Pinard A, Levesque S, Vallee J, et al. Glutamatergic modulation of synaptic plasticity at a PNS vertebrate cholinergic synapse. Eur J Neurosci 2003;18:3241–50
25. Herzog E, Landry M, Buhler E, et al. Expression of vesicular glutamate transporters, VGLUT1 and VGLUT2, in cholinergic spinal neurons. Eur J Neurosci 2004;20:1752–60
26. Kraus T, Neuhuber WL, Raab M. Vesicular glutamate transporter 1 immunoreactivity in motor endplates of striated esophageal but not skeletal muscles in the mouse. Neurosci Lett 2004;360:53–56
27. Boulland JL, Qureshi T, Seal RP, et al. Expression of the vesicular glutamate transporters during development indicates the widespread corelease of multiple neurotransmitters. J Comp Neurol 2004;480:264–80
28. Nishimaru H, Restrepo CE, Ryge J, et al. Mammalian motor neurons co-release glutamate and acetylcholine at central synapses. Proc Natl Acad Sci U S A 2005;102:5245–49
29. Levit TA, Salpeter MM. Denervated endplates have a dual population of junctional acetylcholine receptors. Nature 1981;291:239–41
30. Fumagalli G, Balbi S, Cangiano A, et al. Regulation of turnover and number of acetylcholine receptors at neuromuscular junctions. Neuron 1990;4:563–69
31. Culican SM, Nelson CC, Lichtman JW. Axon withdrawal during synapse elimination at the neuromuscular junction is accompanied by disassembly of the postsynaptic specialization and withdrawal of Schwann cell processes. J Neurosci 1998;18:4953–65
32. Akaaboune M, Culican SM, Turney SG, et al. Rapid and reversible effects of activity on acetylcholine receptor density at the neuromuscular junction in vivo. Science 1999;286:503–7
33. Frank E, Gautvik K, Sommerschild H. Persistence of junctional acetylcholine receptors following denervation. Cold Spring Harb Symp Quant Biol 1976;40:275–81
34. Pun S, Sigrist M, Santos AF, et al. An intrinsic distinction in neuromuscular junction assembly and maintenance in different skeletal muscles. Neuron 2002;34:357–70
35. Goldman D, Brenner HR, Heinemann S. Acetylcholine receptor alpha-, beta-, gamma-, and delta-subunit mRNA levels are regulated by muscle activity. Neuron 1988;1:329–33
36. Ma J, Shen J, Garrett JP, et al. Gene expression of myogenic regulatory factors, nicotinic acetylcholine receptor subunits, and GAP-43 in skeletal muscle following denervation in a rat model. J Orthop Res 2007;25: 1498–505
37. Witzemann V, Brenner HR, Sakmann B. Neural factors regulate AChR subunit mRNAs at rat neuromuscular synapses. J Cell Biol 1991;114: 125–41
38. Adams L, Carlson BM, Henderson L, et al. Adaptation of nicotinic acetylcholine receptor, myogenin, and MRF4 gene expression to long-term muscle denervation. J Cell Biol 1995;131:1341–49
39. Fawcett JW, Keynes RJ. Peripheral nerve regeneration. Annu Rev Neurosci 1990;13:43–60
40. Nishizawa T, Yamashia S, McGrath KF, et al. Plasticity of neuromuscular junction architectures in rat slow and fast muscle fibers following temporary denervation and re-innervation processes. J Muscle Res Cell Motil 2006;27:607–15
41. Osten P, Stern-Bach Y. Learning from stargazin: The mouse, the phenotype and the unexpected. Curr Op Neurobiol 2006;16:275–80
42. Sanford JL, Mays TA, Rafael-Fortney JA. CASK and Dlg form a PDZ protein complex at the mammalian neuromuscular junction. Muscle Nerve 2004;30:164–71
43. Sans N, Racca C, Petralia RS, et al. Synapse-associated protein 97 selectively associates with a subset of AMPA receptors early in their biosynthetic pathway. J Neurosci 2001;21:7506–16
44. Fukata Y, Tzingounis AV, Trinidad JC, et al. Molecular constituents of neuronal AMPA receptors. J Cell Biol 2005;169:399–404
45. Borodinsky LN, Root CM, Cronin JA, et al. Activity-dependent homeostatic specification of transmitter expression in embryonic neurons. Nature 2004;429:523–30
46. Borodinsky LN, Spitzer NC. Activity-dependent neurotransmitter-receptor matching at the neuromuscular junction. Proc Natl Acad Sci USA 2007;104:335–40
47. Spitzer NC, Borodinsky LN. Implications of activity-dependent neurotransmitter-receptor matching. Phil Trans R Soc 2008;363:1393–99
48. Fox MA, Umemori H. Seeking long-term relationship: Axon and target communicate to organize synaptic differentiation. J Neurochem 2006;97: 1215–31

